(This is a sample cover image for this issue. The actual cover is not yet available at this time.)

Biochimica et Biophysica Acta 1818 (2012) 3107–3120

Contents lists available at SciVerse ScienceDirect

Biochimica et Biophysica Acta

journal homepage: www.elsevier.com/locate/bbamem

Comparative study of the AT_1 receptor prodrug antagonist candesartan cilexetil with other sartans on the interactions with membrane bilayers

Charalambos Fotakis [a,b], Grigorios Megariotis [b], Dionysios Christodouleas [a], Eftichia Kritsi [a,b], Panagiotis Zoumpoulakis [b], Dimitrios Ntountaniotis [a,b], Maria Zervou [b], Constantinos Potamitis [b], Aden Hodzic [c,d], Georg Pabst [c], Michael Rappolt [c,*], Gregor Mali [e,f], Johanna Baldus [g], Clemens Glaubitz [g], Manthos G. Papadopoulos [b], Antreas Afantitis [h], Georgia Melagraki [h], Thomas Mavromoustakos [a,**]

[a] Chemistry Department, National and Kapodistrian University of Athens, Panepistimioupolis Zographou 15771, Greece
[b] Institute of Biology, Medicinal Chemistry and Biotechnology, National Hellenic Research Foundation, Vas. Constantinou 48, Athens 11635, Greece
[c] Austrian Academy of Sciences, Institute of Biophysics and Nanosystems Research (IBN), Schmiedlstr. 6, 8042 Graz, Austria
[d] Research Center Pharmaceutical Engineering GmbH, 8010 Graz, Austria
[e] Laboratory for Inorganic Chemistry and Technology, National Institute of Chemistry, Hajdrihova 19, SI-1001 Ljubljana, Slovenia
[f] EN-FIST Centre of Excellence, Dunajska 156, SI-1000 Ljubljana, Slovenia
[g] Institute of Biophysical Chemistry Goethe University Frankfurt, Max von Laue Str. 9, 60438 Frankfurt, Germany
[h] Department of ChemoInformatics, NovaMechanics Ltd, John Kennedy Ave 62-64, Nicosia 1046, Cyprus

ARTICLE INFO

Article history:
Received 22 May 2012
Received in revised form 26 July 2012
Accepted 13 August 2012
Available online 18 August 2012

Keywords:
Candesartan cilexetil
Differential scanning calorimetry
Raman spectroscopy
Small angle X-ray scattering
Solid state NMR
Molecular dynamics

ABSTRACT

Drug–membrane interactions of the candesartan cilexetil (TCV-116) have been studied on molecular basis by applying various complementary biophysical techniques namely differential scanning calorimetry (DSC), Raman spectroscopy, small and wide angle X-ray scattering (SAXS and WAXS), solution ^{1}H and ^{13}C nuclear magnetic resonance (NMR) and solid state ^{13}C and ^{31}P (NMR) spectroscopies. In addition, ^{31}P cross polarization (CP) NMR broadline fitting methodology in combination with *ab initio* computations has been applied. Finally molecular dynamics (MD) was applied to find the low energy conformation and position of candesartan cilexetil in the bilayers. Thus, the experimental results complemented with *in silico* MD results provided information on the localization, orientation, and dynamic properties of TCV-116 in the lipidic environment. The effects of this prodrug have been compared with other AT_1 receptor antagonists hitherto studied. The prodrug TCV-116 as other sartans has been found to be accommodated in the polar/apolar interface of the bilayer. In particular, it anchors in the mesophase region of the lipid bilayers with the tetrazole group oriented toward the polar headgroup spanning from water interface toward the mesophase and upper segment of the hydrophobic region. In spite of their localization identity, their thermal and dynamic effects are distinct pointing out that each sartan has its own fingerprint of action in the membrane bilayer, which is determined by the parameters derived from the above mentioned biophysical techniques.

1. Introduction

Angiotensin II (AngII) receptor blockers (ARBs) are amphiphilic molecules that exert their biological activity by preventing the vasoconstrictive hormone AngII to act on the AT_1 receptor [1,2]. The molecular basis of their antihypertensive action has been interpreted by a two-step model. In the first step they are incorporated into the bilayers through the lipid–water interface and secondly laterally diffuse to reach the active site of the AT_1 receptor in order to exert their biological activity [3–5].

The prodrug 1-[[(cyclohexyloxy)carbonyl]oxy]ethyl, 2-ethoxy-1-[[2′-(1H-tetrazol-5-yl)[1,1′-biphenyl]-4-yl]methyl]-1H-benzimidazole-7-carboxylate denoted as candesartan cilexetil (TCV-116) (see Fig. 1a) is esterified at the carboxyl group by the cyclohexylocarbonyloxyethyl segment of the active compound candesartan (CV-11974) (see Fig. 1b), that belong to sartans antihypertensive drugs [6,7].

The cellular membranes are complex entities consisting of various kinds of proteins and lipids as well as cholesterol. Phosphatidylcholines (PCs) are the most abundant lipid species in the plasma membranes of the vascular smooth muscle cells [8] and sarcolemma cardiac membranes [9]. The most frequently found among them are PCs with oleic and linoleic chains, and further dipalmitoylphosphatidylcholine (DPPC). Hydrated DPPC lipids are used because they spontaneously form multilamellar bilayers whose mesomorphic changes occur in a convenient temperature range between 25 and 50 °C. Their dynamic

* Corresponding author. Tel.: +39 40 375 8708; fax: +39 40 375 8029.
** Corresponding author. Tel.: +30 2107274475; fax: +30 2107274761.
E-mail addresses: michael.rappolt@elettra.trieste.it (M. Rappolt), tmavrom@chem.uoa.gr (T. Mavromoustakos).

0005-2736/$ – see front matter © 2012 Elsevier B.V. All rights reserved.
http://dx.doi.org/10.1016/j.bbamem.2012.08.009

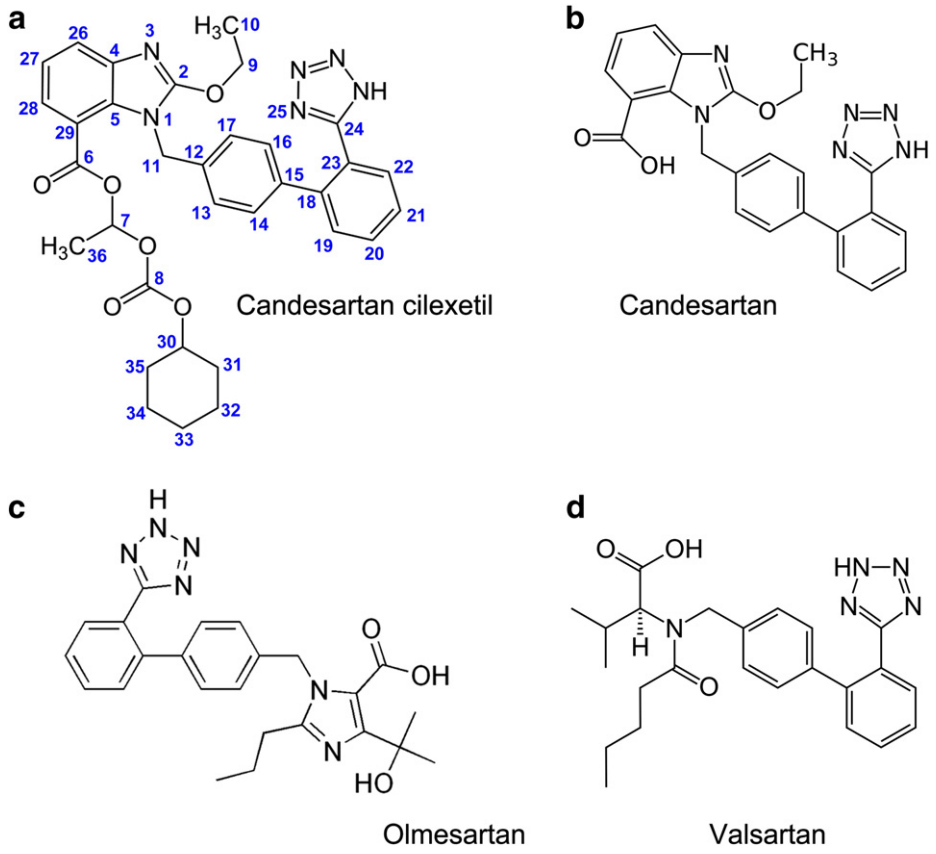

Fig. 1. The chemical structures of (a) candesartan cilexetil, (b) candesartan, (c) olmesartan and (d) valsartan.

and thermotropic properties have been extensively explored [10–19] and their ARB partition coefficient with respect to its aqueous environment [20], especially in the fluid state, resembles that of natural plasma membranes of the vasculature [8,9]. Phosphatidylcholine bilayers at low temperatures occur in the lamellar gel phase ($L_{\beta'}$) and at higher temperatures in the liquid-crystalline phase (L_{α}). The transition is accompanied by several structural changes in the lipid molecules as well as systematic alteration in the bilayer geometry, for example the *trans–gauche* isomerization taking place in the acyl conformation. The average number of *gauche* conformers indicates the effective fluidity, which depends not only on the temperature, but also on perturbation due to the presence of a drug molecule intercalating between the lipids.

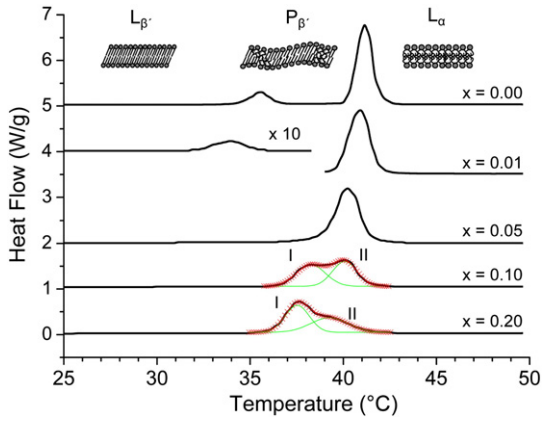

Fig. 2. DSC thermal scans with 2.5 °C/min for samples with different DPPC/candesartan cilexetil (TCV-116) molar ratios. From top to bottom the TCV-116 concentrations are $x = 0$, 0.01 (1 mol% TCV-116), 0.05, 0.10 and 0.20. At 10 and 20 mol% the TCV-116 incorporation splits the main transition into two components (cp. Table 1).

It is more and more evident that drugs affect the lipid membrane core and may induce the formation of microdomains that modulate the activity of proteins, thus offer a new avenue in the membrane-lipid therapy. Representative examples are the drug:membrane interactions of the β2 agonists indacaterol and salmaterol, which are characterized by different pharmacological properties. It was suggested that the synergy between the higher partitioning of indacaterol into microdomains and the faster membrane permeation of indacaterol could explain the faster onset and longer duration of its therapeutic effect with respect to salmaterol. The higher membrane fluidizing effect of salmeterol may contribute to its lower intrinsic efficacy compared to indacaterol [21]. Other studies postulated that active drugs do change the lateral pressure profile in bilayers and hence, can affect the behavior of membrane proteins [22,23]. These are just two examples of the numerous others given in the literature demonstrating that every bioactive molecule can be characterized by its own special fingerprint, when it interacts with membrane bilayers [24].

In this context, our laboratory has initiated research activity to study the effects of the ARBs losartan, valsartan, olmesartan and candesartan in membrane bilayers [3,7,25–27]. Thus, the significant amount of work performed on AT_1 receptor antagonists could also serve for comparative studies and further elaboration of the function of amphiphilic drugs in the cell membrane. In this study, the effects of TCV-116 intercalated in DPPC membranes were investigated, and then were compared with the effects of its active metabolite CV-11974 and other AT_1 receptor antagonists. It is of importance to investigate how the membrane effects of prodrugs are related to their active metabolites in order to understand: (i) if prodrugs administered at the site of action may exert a more beneficial profile than their active metabolites drugs, and to check (ii) if they exert similar or differential, maybe more desirable perturbing effects at the membrane interface.

In the present study an integrated approach using different complementary methodologies has been put into practice, namely differential scanning calorimetry (DSC), Raman spectroscopy, small and wide angle X-ray scattering (SAXS and WAXS), high-resolution liquid nuclear magnetic resonance (NMR) spectroscopy, solid state stationary ^{31}P NMR and ^{13}C cross-polarization magic-angle spinning (CP/MAS) NMR spectroscopy as well as molecular dynamics (MD) have been applied. Further, an in-house CP ^{31}P NMR simulation methodology was implemented that elaborates an automated 7-parameter fitting method and considers the studied DPPC/water multilamellar bilayers immobilized in the time scale of the NMR experiment. A detailed description of the broadline CP ^{31}P NMR simulations of fully hydrated multilamellar DPPC dispersions has been recently published [26,28]. Briefly, DSC provides valuable information on the thermal modifications that are caused by the presence of drugs in the membrane [29]. Raman and X-ray diffraction experiments provide complementary structural information, such as interdigitation effects of the molecules in lipid bilayers [30,31]. Performed solid state NMR experiments included ^{13}C MAS and ^{13}C CP/MAS spectroscopy which offer useful information for the dynamic changes that drugs cause when they are incorporated in the lipid bilayers [32–35]. Typical observations are related with chemical shift or intensity changes of various key atoms which are partitioning in the membrane. Chemical shift changes are further associated with phase transition properties of the membrane bilayer. Moreover new peaks arise because of the presence of the drug. Molecular dynamics (MD) experiments provide useful information on the incorporation, localization and orientation of the drug molecule in the lipid bilayers [36].

2. Materials and methods

2.1. Sample preparation

Dipalmitoyl-phosphatidylcholine (DPPC) was purchased from Avanti Polar Lipids (Birmingham, AL), and used without further purification. Candesartan cilexetil (TCV-116) was kindly provided by Medochemie Hellas A.E. (Pharma Cypria). The preparation of multilamellar vesicles was done as described recently [25]. For DSC experiments portions of ~5 mg from 50% (w/w) liposomal dispersions were used. The same preparation was carried out for the Raman spectroscopy measurements. For X-ray scattering experiments aqueous dispersions of multilamellar vesicles were prepared with a final concentration of 50 mg/mL (5% w/w). For solid state NMR spectroscopy experiments 50% (w/w) liposomal dispersions were used. The drug concentrations used were $x=0.01$ (1 mol% candesartan cilexetil), 0.02, 0.05, 0.10 and 0.20.

2.2. Differential scanning calorimetry (DSC)

The samples obtained as described in the Materials section were transferred to stainless steel capsules obtained from Perkin-Elmer and sealed. Thermal scans were obtained on a Perkin-Elmer DSC-7 instrument (Norwalk, CT). All samples were scanned from 10 to 60 °C at least three times until identical thermal scans were obtained using a scanning rate of 2.5 °C/min. The following diagnostic parameters were used for the study of drug to membrane interactions: T_m (maximum position of the recorded heat capacity), $\Delta T_{m1/2}$ (the full width at half maximum of the phase transition), and the enthalpy change, ΔH. Further experimental details are given in [25].

2.3. Raman spectroscopy

Raman spectra were recorded with a Perkin-Elmer GX Fourier Transform spectrometer (Shelton, CT). A diode pumped Nd:YAG laser at 1064 nm (Norwalk, CT) was used as the excitation source. The scattered radiation was collected at an angle of 180° with respect to the incident beam. Spectra were recorded at a laser power of 400 mW on sample with a resolution of 2 cm^{-1}. Raman spectra of the examined samples were obtained in the frequency region of 3500–400 cm^{-1} and in the temperature range of 25 to 50 °C. Further experimental details are described in [27].

2.4. Small and wide angle X-ray scattering

SAXS experiments were carried out at the Austrian SAXS beamline (Elettra Laboratory, Sincrotrone Trieste, Italy) [37]. A linear one-dimensional gas detector was used covering the q range ($q=4\pi\sin\theta/\lambda$; where 2θ is the scattering angle and $\lambda=1.54$ Å the selected X-ray wavelength) between 0.01 and 0.6 Å^{-1}. Further details on the set-up are found in [25].

Background corrected SAXS patterns were analyzed in the full q-range allowing the application of the modified Caillé theory [38,39]. The bilayer model used and its applications have been recently presented [40]. From the fits to the scattered intensities $I=S(q)\,|F(q)|^2/q^2$ ($S(q)$: structure factor; $F(q)$: form factor) we directly obtained the lamellar repeat distance d and the headgroup-to-headgroup thickness, d_{HH}. The width σ_H of the Gaussian peak applied to model electron density profile of the headgroup region was fixed to 3 Å.

The effective lateral area per molecule was determined from

$$A(x)=\frac{2\cdot V(x)}{d_{Luzzati}(x)}\approx\frac{2\cdot V(x)}{d_{HH}(x)}, \tag{1}$$

where x denotes the TCV-116 concentration. V is the effective molecular volume (see below Eq. (3)) and $d_{Luzzati}$ is the membrane thickness that is defined by the Gibbs dividing surface [41]. Note that for pure PC bilayers in the fluid phase $d_{Luzzati}$ has nearly the same value as d_{HH} [42]. In the case of a linear dependence of $A(x)$ one can extract estimates for the partial molecular areas A_{DPPC} and $A_{TCV\text{-}116}$ by the relation [43]:

$$A(x)=x\cdot A_{TCV-116}+(1-x)\cdot A_{DPPC}. \tag{2}$$

For the studied binary DPPC/TCV-116 formulations the effective volumes were estimated using:

$$V(x)=x\cdot V_{TCV-116}+(1-x)\cdot V_{DPPC} \tag{3}$$

with $V_{TCV\text{-}116}=740$ Å^3 (the bare volume was estimated from losartan's density in the solid state $\rho=1.37$ g/cm^3 and its molecular weight $M_W=610.66$ g/mol), and the values of $V_{DPPC}=1228$ Å^3 ($T=50$ °C) are taken from ref. [42]. Application of the bare volume of candesartan cilexetil assumes that its insertion does not lead to a condensation of the membrane. If condensation takes place, then $V_{TCV\text{-}116}$ is expected to become smaller than 740 Å.

An attempt to estimate computationally the $V_{TCV\text{-}116}$ volume was performed using the semi-empirical quantum chemistry package MOPAC 2009. Before the calculation of the volume, the structure of candesartan cilexetil was fully optimized using the PM6 method included in MOPAC 2009 package [44–46]. The PM6 method was chosen for the geometry optimizations since it offers a good balance between speed and accuracy. A recent paper highlighted the quality of predictions obtained by PM6 method as similar to that of models based on B3LYP [47]. For the optimized structure we have calculated the volume using COSMO included in MOPAC 2009 package. COSMO (COnductor-like Screening MOdel) is a computational method for determining the electrostatic interaction of a molecule with a solvent. COSMO is a continuum approach where the solvent is approximated by a dielectric continuum surrounding the solute molecules outside of a molecular cavity. The method was proven to be computationally efficient and accurate [48]. The calculation of the volume was performed under several environments and different conformations. More specifically, we have first estimated the volume in the presence of gas, water, methanol, DMSO and

chloroform for candesartan cilexetil and the corresponding values were: 717, 731, 730, 733 and 730 Å^3. All these values are very close to the estimation based on the solid state density (740 Å^3) except for the volume measured in the presence of gas. In order to further examine the system, we have continued our study by producing several conformations of candesartan cilexetil using the Balloon software [49]. The average estimated volume in the presence of water for the five first conformations was 736 Å^3 which is very close to the experimental value.

2.5. Nuclear magnetic resonance (NMR) spectroscopy

2.5.1. High resolution liquid NMR

Spectra of candesartan cilexetil were recorded on a Varian 600 MHz spectrometer at 25 °C using a sample concentration of 20 mM. All data are collected using pulse sequences and phase-cycling routines provided in the Varian libraries of pulse programs. Further experimental details and applied protocols are described in [7].

2.5.2. ^{13}C Magic angle spinning NMR spectroscopy

Magic angle spinning (MAS) without or with cross polarization (CP) was carried out on the samples described in the Sample preparation section. The samples were transferred to 3.2 mm zirconia rotors. ^{13}C NMR spectra were obtained at 150.80 MHz with a 600 MHz Varian spectrometer (Palo Alto, CA). The spinning rate used was 5 kHz. The experimental temperatures used were 25 °C, 35 °C, 45 °C for ^{13}C-CP/MAS experiments and 45 °C for the ^{13}C-MAS measurement.

2.5.3. Solid state ^{31}P CP NMR measurements

Solid state ^{31}P CP NMR spectra of DPPC with or without candesartan cilexetil were obtained on a Bruker (Karlsruhe, Germany) MSL 400 NMR spectrometer operating at 161.977 MHz and capable of high-power ^{1}H-decoupling. Each spectrum was an accumulation of 1000 scans. The standard pulse sequence of the Bruker software for the CP experiment was used with the following acquisition parameters: recycling delay 4 s, contact time 5 ms, acquisition time 1 ms, π/2 pulse for proton 7 μs. The contact time was chosen to give optimal spectra after testing at 1, 3 and 5 ms. The temperature range used in the experiments was 25–50 °C. The sample was revolved in a 4-mM rotor at a low frequency of 25 Hz.

2.6. ^{31}P CP NMR simulations

The developed model assumes the lipid molecules to perform fast overall rotational diffusion in both the liquid crystalline and in the more organized gel phase. Both phases exhibit long range orientation order, but the gel phase possesses in addition long range translational order. The latter two properties are intimately related to the concept of the packing quality of the lipids in the bilayer. Overall uniaxial rotations, fluctuations or wobbling of the axis of rotation, internal rotations, and lateral diffusion within the plane of the bilayer are motions of the lipid molecules subjected to the restrictions posed by the anisotropic environment of the bilayer. All simulations were obtained imposing Lorentzian spin packets, and the experimental spectra were simulated by automated fitting using the downhill simplex algorithm with a convergence criterion of 0.01 [26]. The fitting method computes certain parameters from which the following described below were used to extract information regarding the interactions of sartan molecules with the DPPC bilayers.

The isotropic chemical shift, σ_{iso}, is characterized by the chemical shielding tensor which corresponds to the easily recognized average spectral and is defined as the trace of:

$$\sigma_{iso} = \left(\sigma_{xx} + \sigma_{yy} + \sigma_{zz}\right)/3. \quad (4)$$

The inhomogeneous broadening, $\Delta\sigma$, also named the *residual anisotropy* of the chemical shielding (CS) tensor, is related to the internal structure of the polar head group and corresponds to the total width of the broadline. It is indirectly correlated to the orientation obtained by the axis of rotation of the lipids with respect to the CS principal frame. The homogeneous broadening of spin packets, *brd*, is caused by the dipolar ^{1}H–^{31}P interaction of the phosphorous with the neighboring methylene protons. The collective tilt angle, Θ_{DR}, was determined by the director *D*, and the long axis of the phospholipid molecules. This angle refers to the collective tilt of the lipids and is related to the long-range orientational order of the bilayer. For further details refer to [26].

2.7. Molecular dynamics of lipid bilayers

A bilayer of 72 DPPC molecules was simulated in the full-atom representation under the CHARMM 36 force field [50,51], in contact with a water phase of 2162 water molecules described by the TIP3P [52] (transferable intermolecular potential 3P) model. An equilibrated structure of the bilayer was provided as a PDB file by the Laboratory of Molecular and Thermodynamic Modeling at University of Maryland. Regarding to the candesartan cilexetil prodrug, its topology file was made with the SwissParam server program [53] that provides topology files in GROMACS format, based on Merck molecular force field (MMFF) [54] in a functional form that is in compatibility with the CHARMM force field. It is also worth mentioning that MMFF reproduces accurately bond lengths, bond angles and vibrational frequencies in comparison with experimental data [53,54]. An additional reason for choosing the above-mentioned server was the extensive successful tests reported in reference [53] about small organic molecules into biomolecules which were described by CHARMM force field [55]. All simulations were performed with the molecular dynamics package GROMACS 4.5.4 (see ref. [54] and therein) in the NPzAT ensemble with a constant area per lipid, *A*, equal to 0.64 nm^2/lipid whereas the equations of motion were integrated with a time step equal to 2 fs. Temperature was kept constant at 50 °C using the Berendsen thermostat [56] with a coupling time constant equal to 0.1 ps whereas the Berendsen barostat [56] was employed for the pressure coupling along the *z*-axis at 1 bar with a coupling time constant equal to 1 ps. As far as the long range electrostatic interactions are concerned, they were treated with the particle mesh Ewald (PME) method [57] while Coulomb and Lennard–Jones interactions were calculated using a 1.0 nm cut-off radius. The system was initially energy-minimized using the steepest descent method and after that the MD simulation was started. The duration of the MD simulation equals to 120 ns while the last 40 ns were used for the computation of the selected properties.

The potential of mean force (PMF) of the candesartan cilexetil from water to lipid phase was computed by a set of *umbrella sampling simulations* with the reaction coordinate, ζ, to be the *z*-axis ($\zeta = 0$ for the bilayer center). To this end, a harmonic potential ($k = 500$ kJ/mol/

Table 1
Thermodynamic parameters of pure DPPC and with candesartan cilexetil (TCV-116) incorporated at molar ratios of $x = 0.01$ (1 mol% TCV-116), 0.05, 0.10 and 0.20. Total main transition enthalpies are given in bold.

Samples	T_{pre} (°C)	ΔT_{pre} (°C)	ΔH_{pre} (kcal/mol)	T_m (°C)	ΔT_m (°C)	ΔH_m (kcal/mol)
DPPC (x = 0.0)	35.5	1.0	1.20 ± 0.03	41.2	1.0	**7.89** ± 0.08
DPPC/TCV-116 ($x = 0.01$)	33.9	1.8	0.28 ± 0.04	40.5	1.15	**7.88** ± 0.08
DPPC/TCV-116 ($x = 0.05$)	–	–	–	40.1	1.33	**8.61** ± 0.09
DPPC/TCV-116 ($x = 0.10$)	–	–	–	I: 38.3 II: 40.1	1.6 1.3	4.53 ± 0.04+ 4.44 ± 0.04= **8.97** ± 0.09
DPPC/TCV-116 ($x = 0.20$)	–	–	–	I: 37.5 II: 39.2	1.3 2.0	5.44 ± 0.05+ 4.53 ± 0.04= **9.97** ± 0.10

nm^2) was imposed on the center of mass of the drug and thirty three windows were used for the biasing molecular dynamics simulations. The distance for each window was defined between the centers of mass of the bilayer and drug. In particular, the PMF was computed by the weighted histogram analysis method (WHAM) [58,59] that is available in GROMACS. These computations were done in an extended system that contains 3020 water molecules so as to avoid the interaction of the drug with the periodic image of the opposite leaflet of the bilayer. The protocol we followed is according to the umbrella sampling simulations reported in references [60,61]. The duration of the thirty three biasing simulations is 20 ns in which the first 5 ns are regarded as equilibration while the rest parameters are exactly the same with those reported in the previous subsection. Preferable configurations of the candesartan cilexetil in the DPPC bilayer were determined applying a clustering algorithm that is available in the UCSF Chimera software [62].

3. Results

3.1. Differential scanning calorimetry

The thermal changes in the pure DPPC/water system as well as the influence of different concentrated inclusions of TCV-116 in DPPC bilayers are shown in Fig. 2. In pure DPPC (top curve) two characteristic endothermic peaks are visible referring to the pre- and the main transition, respectively. The DPPC molecules form below the pre-transition the well organized lamellar gel phase, $L_{\beta'}$, while above the main transition temperature the fluid lamellar phase, L_{α}, is apparent. An intermediate phase, $P_{\beta'}$, is also observed, in which the bilayers are modulated by a periodic ripple (ripple phase). The recorded transition temperatures and enthalpies are in good agreement with literature values [10] (Table 1). The insertion of TCV-116 at 1 mol% almost abolishes the pre-transition and shifts it to a lower temperature. It affects also the main transition by increasing its width and shifting it to a lower temperature by 0.7 °C (Table 1). The presence of TVC-116 at this low concentration affected only the enthalpy change; ΔH, of the pre-transition by lowering its value about 4 times. When 5 mol% of the prodrug is incorporated, the pre-transition was abolished and the main transition was further shifted to lower temperature while its width further increased. TVC-116 at this concentration caused a ΔH increase of the main phase transition (Table 1). At higher concentrations (10 and 20 mol%) TVC-116 caused extensive broadening of the phase transition with two distinct maxima (at T_I and T_{II}) and a further increase of the total enthalpy, ΔH, of the main phase transition (Table 1).

3.2. Raman spectroscopy

Raman spectra of pure DPPC bilayers in the presence of 20 mol% TVC-116 were obtained in a temperature range of 27–50 °C. The transition behavior was especially characterized by the C–H and C–C stretching modes changes.

The C–C stretching mode region in the spectral interval of 1050–1150 cm^{-1} reflects directly intramolecular *trans–gauche* conformational changes within the hydrocarbon chain region of the lipid matrix [17,18]. Fig. 3a shows the changes in the $I_{1090/1130}$ intensity ratio caused by TVC-116 when incorporated into DPPC bilayers. The transition temperatures of pure DPPC bilayers compare well to the results found from the calorimetric measurement (cp. Fig. 2, Table 1), however, at $x = 0.20$ the two main transition components, at T_I and T_{II}, are not resolved by the $I_{1090/1130}$ intensity ratio, instead a rather continuous increase in the $I_{1090/1130}$ intensity ratio is observed. The effect of TVC-116 is quite significant: first, the fluidity in the gel phase is slightly increased (from about 0.68 to 0.78), and secondly, the *trans* to *gauche* isomerizations change strongly, *i.e.* the intensity ratio drops from 1.5 to 0.9 at 50 °C (60% decrease).

The most intense bands in the Raman spectrum are those attributed to the methylene C–H stretching mode region from 2800 to 3100 cm^{-1}. In particular, the symmetrical and antisymmetrical methylene stretching bands allow investigating phase transition behaviors. The intensity ratio of these two bands $I_{2845/2880}$ describes the main changes occurring in the hydrocarbon chain region. This ratio is sensitive to subtle changes in conformational order from rotations, kinks, twists and bends of the lipid chains [63]. Similar to the findings for the $I_{1090/1130}$ ratio, in the gel phase regime the $I_{2845/2880}$ values are slightly higher with the intercalation of the drug, but the intensity ratio is clearly reduced in the fluid phase regime in the presence of TVC-116 indicating a strong reduction in chain disorder (Fig. 3b). The intermolecular lipid chain interactions of the lipids can be elicited from changes in the 2935/2880 peak height intensity ratio that measures the effects originating from changes both in interchain order and intrachain order–disorder processes. The $I_{2935/2880}$ ratio constitutes a sensitive probe to monitor the lipid phase transitions despite the fact that the C–H stretching mode region consists of many superimposed vibrational transitions [64–66]. In the pure DPPC dispersion, again the pre- as well as main transitions are clearly displayed

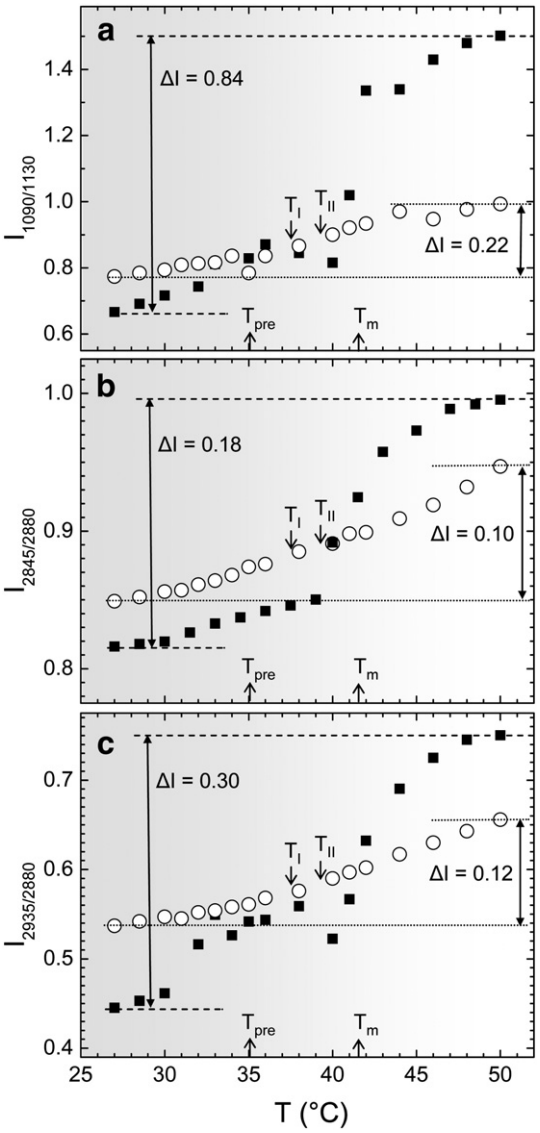

Fig. 3. (a) $I_{1090/1130}$ ratio *vs.* temperature plots for pure DPPC (solid squares) and DPPC containing $x = 0.20$ of candesartan cilexetil (open circles) are shown. In panel (b) the corresponding $I_{2850/2880}$ and (c) the $I_{2935/2880}$ ratios are depicted. The pre-transition temperature, T_{pre}, and main transition temperature, T_m, are marked with arrows on the abscissa, while the transition temperatures, T_I and T_{II} for the DPPC/TCV-116 sample are marked on the respective plots (cp. Fig. 2 and Table 1).

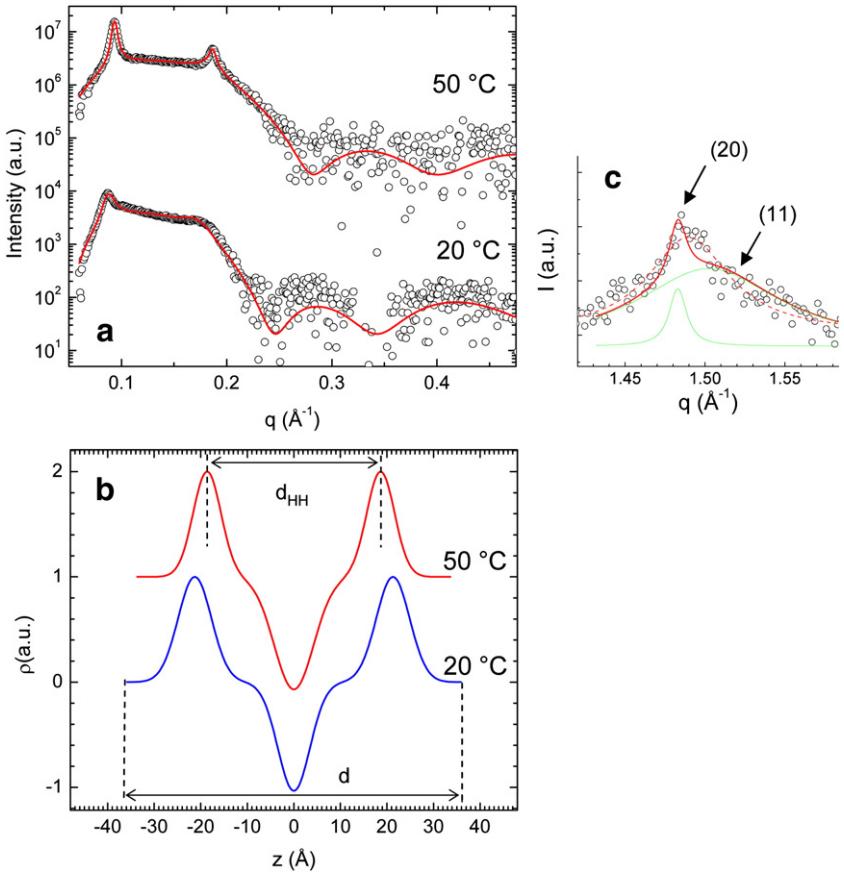

Fig. 4. X-ray scattering curves of DPPC/TCV-116 multilamellar vesicles at 20 °C and 50 °C (a), and their corresponding electron density profiles (b). In panel c the WAXS peak arising from the hexagonal chain packing is plotted. The full red lines in panels a and c give the best fit to the data (cp. Table 2). (For interpretation of the references to color in this figure legend, the reader is referred to the web version of this article.)

(Fig. 3c). In contrast, in the presence of the prodrug TVC-116 only a smooth and monotonous increase of $I_{2935/2880}$ can be seen. Also the overall intensity changes, ΔI, are far smaller ($\Delta I = 0.30$ compares to $\Delta I = 0.12$; Fig. 3c).

Other characteristic band alterations give evidence for the incorporation of TCV-116 in the DPPC bilayers (data not shown). First, an additional band around 1600 cm^{-1} was observed, which is attributed to the aromatic C=C stretch. The above mentioned band was observed also in bilayers containing the AT_1 receptor antagonist CV-11974. The presence of additional aromatic peaks characteristic of their incorporation was observed for CV-11974 (Fig. 1b) at 800 cm^{-1} and at 1024 cm^{-1} for olmesartan (Fig. 1c), another member of the sartans family [7,27]. Second, the band at 714 cm^{-1} corresponding to C–N stretch vibration, showed a shift to higher values, when TCV-116 is present in the membrane. This indicates that TCV-116 interacts with headgroups. Third, TCV-116 caused a shift and line-shape changes at 1296 cm^{-1} which correspond to stretching vibrations of the (CH_2) region of the DPPC bilayers. This is a direct evidence of the interaction of TCV-116 with (CH_2) region of the DPPC bilayers.

3.3. Small and wide angle X-ray scattering

In Fig. 4 are shown the scattering patterns of DPPC bilayers in the presence of $x = 0.2$ TVC-116 at 20 and 50 °C, respectively. As commonly observed for sartans [25,27] an increased stacking disorder in the multilamellar vesicles (MLVs) is observed also in the presence of TVC-116. This disorder is stronger in the gel-phase. In the bottom scattering pattern of Fig. 4a (20 °C), mainly form factor contributions are present accompanied only by a weak first order diffraction peak at $q = 0.08$ Å^{-1}. Both SAXS patterns have been analyzed by global fitting procedures [19], and best fits are displayed by solid red lines. The corresponding electron density profiles are displayed in Fig. 4b, and the most important structural parameters as well as the membrane fluctuation parameter σ are summarized in Table 2. Note that for the gel phase σ(gel) is deduced from the paracrystalline theory for lattice disorder of second type [67], *i.e.* practically flat bilayers are considered to oscillate with respect to the neighboring membranes, while for the fluid phase σ(fluid) [68] is deduced from the application of the modified Caillé theory [38,39]. In the later theory also bilayer

Table 2
Structural data on pure DPPC bilayers and DPPC membranes with 20 mol% ($x = 0.2$) candesartan cilexetil (TCV-116), respectively.

	DPPC (20 °C)	DPPC (50 °C)	DPPC/TCV-116 (20 °C)	DPPC/TCV-116 (50 °C)
d (Å)	63.5[a]	67.0[a]	71.8	67.3
d_{HH} (Å)	44.2[a]	38.3[a]	43	37
d-d_{HH} (Å)	19.3[a]	28.7[a]	29	30
A (Å^2)	47.9 (20.3)[a]	64[a]	48[b] (20.5)	64/46[c]
σ (Å)	1[d]	6[e]	8	8

[a] Structural data taken from the review [42].
[b] The area per lipid in the gel phase was calculated under the assumption of a chain conserved chain tilt.
[c] The partial areas A_{DPPC} and $A_{TCV\text{-}116}$ were obtained applying Eq. (2) and refer to Fig. 5d.
[d] Estimated values from the global data analysis applying the paracrystalline theory.
[e] Data concerning the root mean square fluctuation in pure DPPC rely on data from references [68,75].

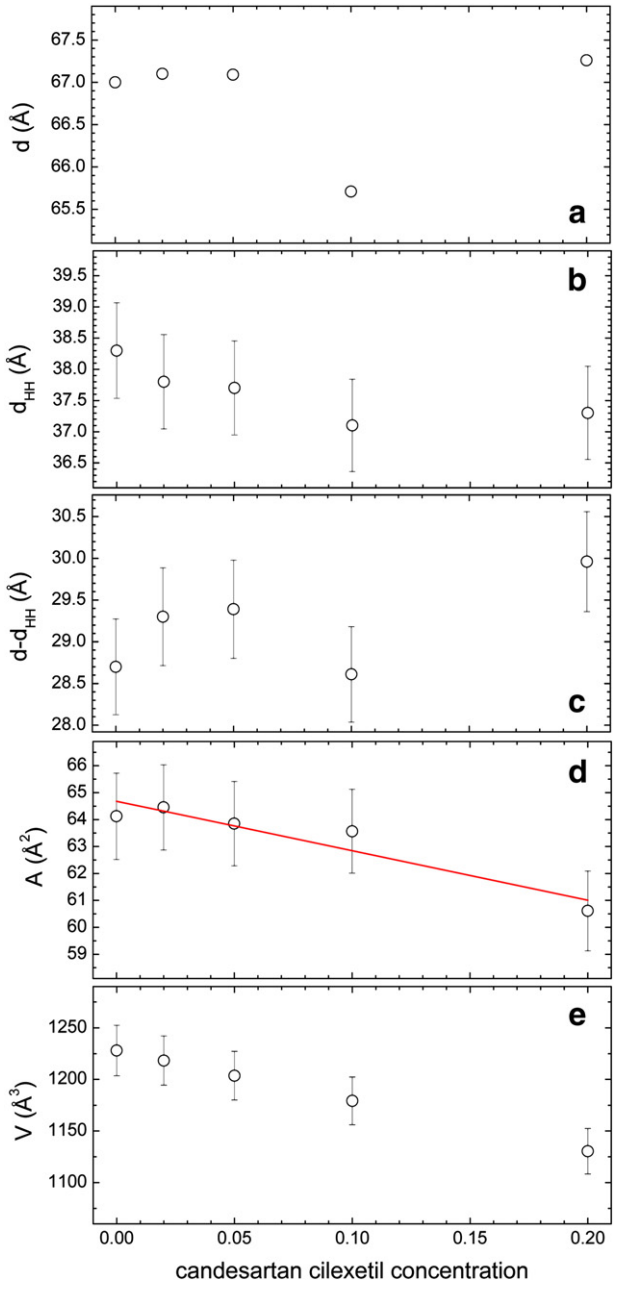

Fig. 5. Bilayer parameters of DPPC at 50 °C in dependence of candesartan cilexetil concentration. a: *d*-spacing, b: head to headgroup distance, d_{HH}, c: water layer thickness, d-d_{HH}, d: effective area per molecule, *A*, and e: effective molecular volume.

undulations are included. The most obvious alterations caused by candesartan cilexetil are the loose stacking in the gel-phase as evidenced by the large interstitial water layer ($\Delta(d\text{-}d_{HH}) = +9$ Å and $\Delta\sigma = +7$ Å; Table 2) and the enhanced diffuse scattering due to positionally uncorrelated membranes (unbound state). The lipid chain packing area A_C at 20 °C was retrieved from the (20) and (11) reflections according to Sun et al. [69]. The fitted *d*-values $d_{20} = 4.24$ Å and $d_{11} = 4.18$ Å compare well to the literature values found for pure DPPC [69], however, the expected orthogonal chain packing is not undoubtedly expressed in the diffraction pattern, and hence we alternatively fitted also a single Bragg peak centered at $q = 1.5$ Å^{-1} (Fig. 4c). In both cases the determined chain packing area A_C is virtually the same as for pure DPPC bilayers (Table 2). This also holds true for the area per lipid, but only under the assumption of conserved chain tilt. In the fluid phase the bilayer swelling and increase of membrane fluctuation parameter are less pronounced ($\Delta(d\text{-}d_{HH}) = +1.3$ Å and $\Delta\sigma = +2$ Å; Table 2).

Further, the influence of candesartan cilexetil in the fluid phase at 50 °C was examined in a concentration range from $x = 0$ to 0.20. The main results from the SAXS experiments are given in Fig. 5. Apart from the interbilayer distance at 10 mol% drug concentration all other derived structural results follow monotonous trends as a function of *x*. The induced membrane thinning from 38.3 to 37.0 Å ($\Delta d_{HH} \sim 1.5$ Å; Fig. 5b) is accompanied by a steady increase in the water spacing, d-d_{HH} (Fig. 5c). Also the effective area per molecule, *A*, displays an almost linear behavior (Fig. 5d). This suggests that candesartan cilexetil does not affect the lateral area of DPPC significantly and allows us to estimate the partial molecular areas for DPPC and candesartan cilexetil applying Eq. (2) (solid line in Fig. 5d). A_{DPPC} results in 64 Å$^2 \pm 1$ Å^2 and $A_{TCV\text{-}116} = 46 \pm 3$ Å^2. A_{DPPC} is well in agreement with literature data [42]. In Fig. 5e the estimated effective volumes per molecule are shown. They are calculated from the partial volumes as specified in the Material and methods section.

3.4. NMR spectroscopy

3.4.1. High resolution liquid NMR profile

TCV-116 was dissolved in deuterated dimethyl sulfoxide solvent (d6-DMSO) that provides an amphiphilic environment reported to mimic the physiological environment of membrane bilayers [70]. The structure elucidation of TCV-116 is required for two reasons: (i) it confirms the purity and identity of the prodrug under study; (ii) it explains the additional ^{13}C signals in the ^{13}CP/MAS experiments attributed to the incorporation of the drug.

The unambiguous drug structure identification of TCV-116 has been achieved using 1D and 2D homonuclear and heteronuclear NMR experiments (see in Supplementary Materials Fig. S1 and Table S1 as well as a brief description), and previous reported work on the structural and conformational analysis of other AT_1 receptor antagonists, especially candesartan (CV-11974) and synthetic analogs [7,71–73].

3.4.2. ^{13}C Magic angle spinning NMR spectroscopy

To obtain detailed local information on the incorporation of candesartan cilexetil in the DPPC bilayers, high-resolution solid-state NMR spectroscopy was applied using magic angle spinning (MAS) with and without cross polarization (CP).

In Fig. 6 the CP-MAS spectra are displayed for 25, 35 and 45 °C. Each spectrum is divided into three regions, namely referring to the carbon atoms in the (i) hydrophobic region (10–40 ppm), to those in (ii) headgroup, glycerol backbone regions and region containing carbons between aromatic segments (55–80 ppm) and (iii) to the aromatic and esterified carbonyls (125–180 ppm).

At 25 °C, candesartan cilexetil caused a significant broadening in the line width of the observed peaks. In addition, some broad and barely observable peaks are detected in the aromatic region, which reflects the incorporation of candesartan cilexetil in the DPPC bilayers. This significant broadening in the presence of candesartan cilexetil results in the absence of features commonly seen in the aliphatic peaks resonated between 14 and 33 ppm. At 35 °C, the same conclusions can be derived. At 45 °C the specimen of DPPC/TCV-116 bilayers again displays a set of broad peaks that resemble those of the lamellar gel phase and ripple phase. In contrast, the pure DPPC bilayers show the well known sharpening of all the peaks as the temperature is greater than T_m. We note that the MAS spectrum at 45 °C without cross polarization was not informative, since the samples of DPPC alone and DPPC/TCV-116 provided almost identical spectra (see Supplementary Materials, Fig. S2). Table S2 (Supplementary Materials) shows in detail the observed chemical shifts for DPPC

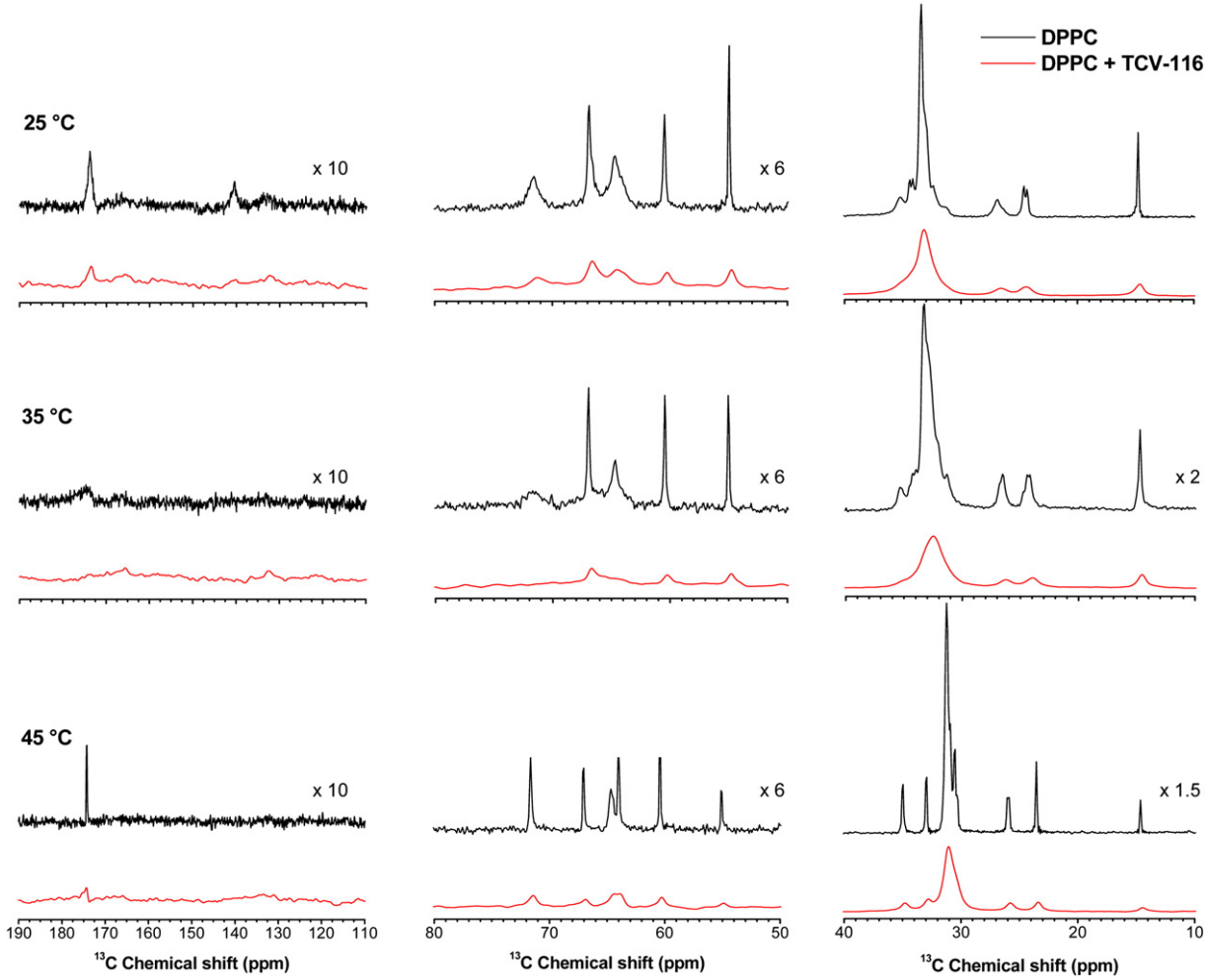

Fig. 6. ^{13}C-CP MAS spectra at 25 °C, 35 °C and 45 °C for pure DPPC (black lines) and DPPC/TCV-116 bilayers (red lines: 20 mol% TCV-116). (For interpretation of the references to color in this figure legend, the reader is referred to the web version of this article.)

and changes that are caused by the incorporation of TVC-116 in the ^{13}C-CP/MAS and ^{13}C-MAS experiments. This includes listings of the additional peaks attributed to candesartan cilexetil.

3.5. Simulations of broadline ^{31}P NMR spectra

Experimental and simulated ^{31}P NMR spectra of DPPC and DPPC loaded with candesartan cilexetil bilayers have been obtained at ascending 2 °C in the temperature range of 25–50 °C (Fig. 7). Several conclusions can be drawn by studying the experimental and simulated spectra. The presence of the prodrug in the lipid bilayers (Fig. 7b) has as a consequence (i) the modification of the isotropic shift toward lower values and (ii) the abolishment of the deep minimum observed in the ^{31}P NMR broadline spectra in gel phase. This minimum is especially prominent in pure DPPC bilayers above 30 °C (Fig. 7a). (iii) The profiles of the spectra containing the prodrug do not change significantly with the temperature.

The spectral simulation parameters of unloaded and loaded DPPC bilayers in the range of 25–50 °C are summarized in Table S3 (Supplementary Materials), and their temperature profiles are further plotted in Fig. 8 in order to extract information regarding dynamical and conformational characteristics of the bilayers that are affected by the incorporation of the drug. In particular, as presented in Fig. 8a, the incorporation of TCV-116 molecules significantly decreases the isotropic chemical shift, σ_{iso}, due to the extra shielding provided to the ^{31}P bilayer polar head.

In Fig. 8b the effect of TCV-116 on the inhomogeneous broadening, $\Delta\sigma$, is shown. Unloaded DPPC bilayers exhibit a significant reduction of $\Delta\sigma$ in the range of 27–32 °C and a change in the slope at 33 °C (a value that is close to the pre-transition temperature; cp. Fig. 2; Table 1) suggesting the transition to another phase. Above 33 °C the value of this parameter remains constant. The incorporation of TCV-116 molecules differentiates the trend of this parameter indicating that the prodrug molecule disturbs the conformation of the headgroup. The values of $\Delta\sigma$ are significantly higher in the case of sartan loaded bilayers up to 43 °C. Above 43 °C the two preparations have comparable $\Delta\sigma$ values.

The homogeneous broadening temperature profile (*brd*; Fig. 8c) of unloaded bilayers decreases monotonically in the temperature range of 25–35 °C indicating a significant increase of the mobility of the bilayer as temperature increases. In the preparation containing TCV-116 the decrease is monotonous but not as steep. In addition, the homogeneous broadening values above 33 °C are always higher than the respective ones containing no prodrug. In the liquid crystalline state the *brd* values of the DPPC/TCV-116 preparation are significantly lower as compared to the ones of pure DPPC bilayers.

The temperature profiles of collective tilt, Θ_{DR}, of unloaded and loaded bilayers are displayed in Fig. 8d. The changes in the slope of these profiles occur approximately at 35 °C and 43 °C (values close to the pre-transition and the main transition temperature, respectively; cp. Fig. 2 and Table 1), thus ascertaining the existence of three lamellar phases. In the temperature range of 25 to 33 °C and 43 °C to 50 °C the Θ_{DR} values of unloaded bilayers are higher in comparison

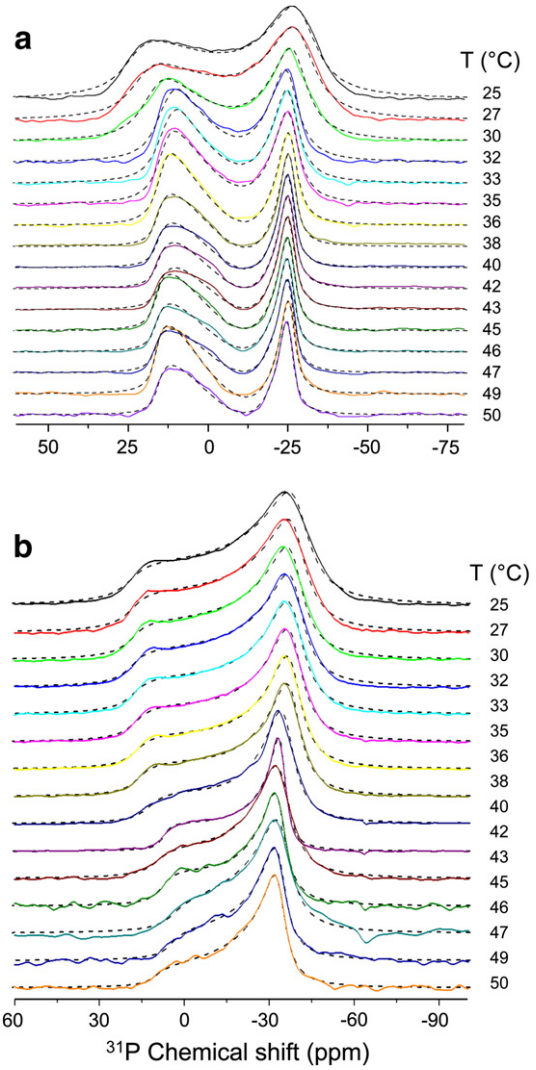

Fig. 7. Experimental (solid lines) and simulated (dashed lines) ^{31}P NMR spectra of DPPC bilayers alone (a) and with candesartan cilexetil ($x = 0.2$) (b) in the temperature range of 25–50 °C.

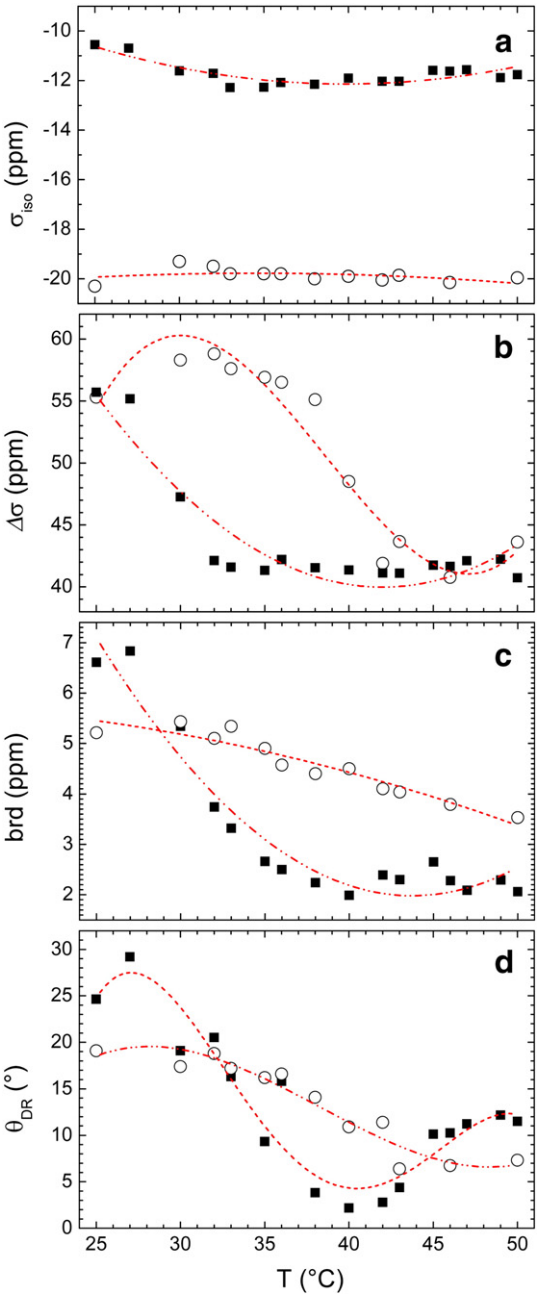

Fig. 8. Temperature dependence of the key fitting parameters of the ^{31}P NMR spectra of pure DPPC bilayers (solid squares) and DPPC membranes with candesartan cilexetil ($x = 0.2$) (open circles) in the temperature range of 25–50 °C: (a) Isotropic chemical shift, σ_{iso}, (b) residual anisotropy, $\Delta\sigma$, (c) homogeneous broadening, *brd*, and (d) collective tilt angle, Θ_{DR}. Note, the dashed red lines (polynomials) are only given to guide the eye. (For interpretation of the references to color in this figure legend, the reader is referred to the web version of this article.)

to the loaded bilayers. However, from 33 °C to 45 °C the bilayers containing TCV-116 have higher values.

3.6. Molecular dynamics

Our analysis starts with the density profiles of all components along the *z*-axis which is normal to the two DPPC leaflets. The TCV-116 was placed initially in the water phase and in the course of the simulation, it penetrated into the bilayer. The exact distribution of all components is given in Fig. 9a, in which it is clear that the drug prefers being in the interior of the DPPC bilayer. Within a simulation time of 40 ns the distance of the drug center with respect to the bilayer center is in average 1 nm (Supplementary Materials, Fig. S3). Furthermore, this way crossing events can be checked (*i.e.*, the migration of the drug from the one leaflet to the other) during the course of the simulation. In this case, the drug did not cross through the middle of the bilayer to reach the opposite leaflet.

As described in the Materials and methods section, umbrella sampling simulations were conducted in order to compute the potential of mean force (PMF) of the candesartan cilexetil from the water to lipid phase (see Supplementary Materials Fig. S4). In accordance with the mass density profile of candesartan cilexetil (Fig. 9a), the global minimum is found at 1 nm distance from the bilayer midplane. Note that the drug was initially placed in the water phase and then penetrated to the position indicated by the PMF. Another interesting observation is the energy barrier (+14.7 kJ/mol) around the middle of the bilayer that has to be overcome from candesartan cilexetil to reach the opposite leaflet. In addition, the free energy for partitioning into the membrane was computed by the difference of PMF at large distances and at the location of the minimum. This value is approximately equal to −50.7 kJ/mol. Also, there is a linear region in the PMF, which is characterized by a large attractive force toward the interior of the bilayer, and its slope equals to 37.6 kJ/mol/nm. The aforementioned region ends at a constant value of PMF that corresponds to the water phase which is not affected by the presence of the bilayer.

Besides, it should be noted that the there is no cylindrical confinement in the drug during the umbrella sampling simulations. In general, cylindrical confinement leads the molecule to adopt less number of states, increasing thus the accuracy of the estimated free energy profile. An excellent study for umbrella sampling simulations of molecules in a lipid bilayer is given in reference [74].

Due to the position of the drug in the bilayer, it is expected a strong interaction with the DPPC–water interface through hydrogen bonds. Indeed, there are hydrogen bonds between the TCV-116 and the other components of the system (water and DPPC) and particularly the number of hydrogen bonds with DPPC and water is 0.633

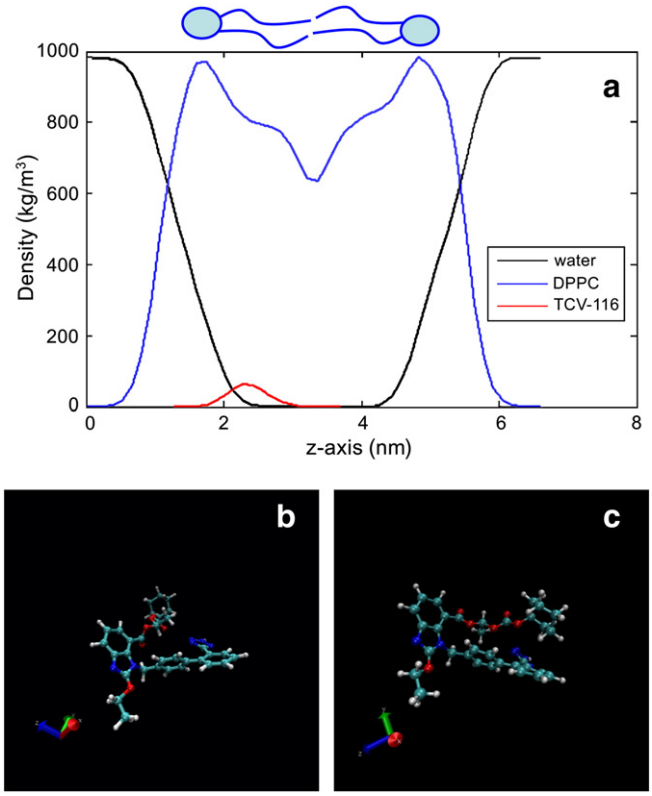

Fig. 9. Molecular dynamics simulation on the interaction of candesartan cilexetil with DPPC bilayers. (a) Mass density profiles of water (black), DPPC bilayers (blue) and candesartan cilexetil (TCV-116) (red) are presented. On top two representative lipid molecules of the bilayer are depicted schematically. Most representative structures of the candesartan cilexetil in the DPPC membrane are shown in panels B and C. The membrane plane is parallel to the *x*, *y*-axes, *i.e.* its normal coincides with the *z*-axis. (For interpretation of the references to color in this figure legend, the reader is referred to the web version of this article.)

and 2.151, respectively. The most preferable conformations of the TCV-116 in the DPPC bilayer are depicted in Fig. 9B and C. Here two representative conformers are depicted in decreasing order.

4. Discussion

4.1. Lipid conformational changes and formation of domains

The phase behavior of pure DPPC is very well documented [75]. Briefly, multilamellar vesicles of DPPC in excess of water undergo an endothermic melting transition, in which the van der Waals interaction energy accounts for 63% of the total enthalpy and changes in rotamer energy amount to 32% [76]. The intermediate ripple phase formation is commonly related to the coexistence of alternating fluid- and gel-like domains [77,78], but alternative models describing the $P_{\beta'}$ phase built up by a single gel phase have also been put forward [79].

The most striking result of the DSC experiments is that the main transition splits into two components at high TCV-116 concentrations ($x = 0.10$ and 0.20), which is most probably caused by the formation of prodrug rich and poor domains. Interpreting the incorporation of the prodrug as a membrane impurity, it is most likely that the low temperature component (I) is caused by the melting of TCV-116 rich domains, whereas the higher temperature component (II) is due to the melting of TCV-116 poor domains (Fig. 2, Table 1). This view is supported by the fact that the enthalpy of component (I) becomes dominant at the highest drug concentration. A very similar behavior was found also for losartan [3,80], irbesartan [81], and valsartan [25], whereas olmesartan [27] and the CV-11974 [7] do not induce any splitting of the main transition. Moreover, the latter two sartans are not able to suppress the pre-transition (up to $x =$ 0.20), while all other studied sartans do suppress the pre-transition above a drug concentration of 5 mol% [3,25,80,81]. This also means that olmesartan and candesartan are not disturbing the lipid chain packing in the gel-phase significantly.

As expected from calorimetric measurements TCV-116, as also losartan [7] and valsartan [25], influences significantly the analyzed Raman ratios (Fig. 3). Interestingly, all three molecules: (i) do not display the pre-transition anymore; (ii) show slightly bigger ratios in the gel-phase and (iii) significantly smaller ratios in the fluid-phase as compared to pure DPPC vesicles. Referring to the *gauche/trans* ratio ($I_{1090/1135}$; Fig. 3A) this means that losartan, valsartan and TCV-116 enhance the bilayer fluidity below the melting point, but decrease it above T_m. Noteworthy, among all studied sartans TCV-116 shows the strongest ability to reduce the *gauche/trans* ratio in the L_α phase (see that $\Delta I_{1090/1130}$ drops from 0.84 to 0.22; Fig. 3A). On the contrary, the Raman ratios of candesartan (CV-11974) [7] concerning the *gauche/trans* ratio and chain mobility (reflected in $I_{1090/1135}$ and $I_{2935/2880}$, respectively) do clearly display the pre-transition. Candesartan has also little effect on the absolute values of the Raman ratios in the gel-phase regime. However, the fluidity of the bilayers in the L_α phase reduces significantly ($\Delta I_{1090/1130}$ drops from 0.84 to 0.38). Similarly olmesartan does not disturb the chain packing in the $L_{\beta'}$ phase, which was confirmed by wide angle X-ray scattering (WAXS) data [27], *i.e.*, the common lipid chain packing on an orthogonal lattice is unaltered [69]. However, olmesartan [27] seems so far the only sartan that is able to increase the fluidity above the melting point, presumably because its polar interactions are weakened due to possible intermolecular hydrogen bonding between the carboxylate and hydroxyl groups.

A further hint for TCV-116's ability to induce the formation of domains at high drug concentrations (Fig. 2; $x = 0.1$ and 0.2) is provided by the wide angle X-ray diffraction (WAXD) data. In Fig. 4C the recorded wide angle peaks reflect the lipid chain packing in the gel-phase, but WAXD pattern at 20 °C displays neither a clear symmetric (hexagonal packing) [82] nor a convincing pattern typical for a chain packing on an orthogonal lattice [69]. Thus, the chain packing known from the pure $L_{\beta'}$ phase [69] is not completely conserved, when TCV-116 is incorporated into the bilayer. Recently, we reported on similar effects found for the addition of valsartan [25]. Here the chain packing appears on a hexagonal lattice, and further, the SAXS pattern suggested the coexistence of bilayers with fully interdigitating non-tilted chains ($L_{\beta I}$ phase) with bilayer domains that conserve the $L_{\beta'}$ phase.

4.2. Prodrug-induced structural changes in the lipid bilayer

Even though DSC and WAXS data suggest the formation of TCV-116 poor and rich domains, respectively, this is not confirmed by the SAXS data experiments. The data analysis of the SAXS pattern at 20 °C indicates no drastic membrane thickness heterogeneity

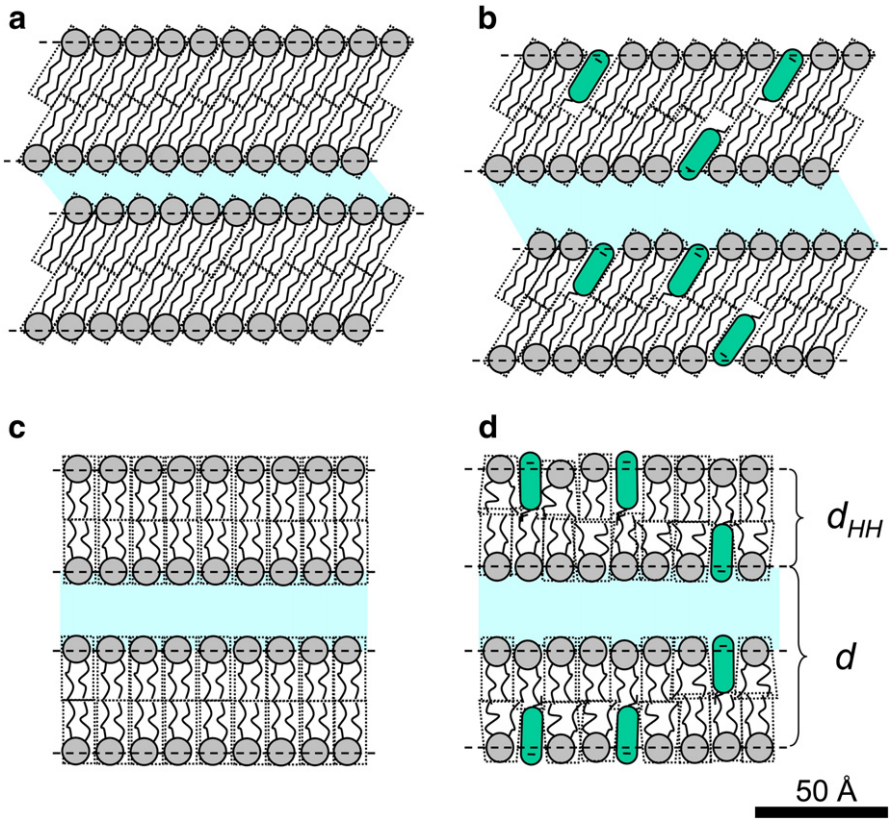

Fig. 10. Schematic illustration of DPPC bilayer structure alterations induced by candesartan cilexetil (TCV-116). Without the drug the $L_{\beta'}$ phase is present at 20 °C (a). The incorporation of 20 mol% TCV-116 induces a significant swelling of the $L_{\beta'}$ phase (b). Panel c demonstrates pure DPPC bilayers in the L_α phase at 50 °C. The same conditions with 20 mol% TCV-116 are given in panel d. Dimensions in all panels base on the structural data given in Table 2.

(Fig. 4a and b, bottom curves). The global fit is well compatible with one bilayer thickness only, *i.e.*, the obtained bilayer thickness d_{HH} = 43 Å is almost the same as found for pure DPPC (Table 2). This in turn means that the prodrug-rich domains are unlikely to resemble a fully interdigitated lamellar $L_{\beta I}$ phase (d_{HH} ~ 35 Å). However, the observed increase in the main transition enthalpy at 20 mol% TCV-116 (Table 1), which is in the same order of magnitude as for losartan [3,80] and valsartan [25], would instead support the assumption, that also TCV-116 mediates at least partially chain interdigitation in the gel-phase. This is supported by the fact that the enthalpy of the interdigitated $L_{\beta I}$ to L_α phase transition is about 1 kcal/mol bigger as compared to $L_{\beta'}$ to L_α phase transition in PC systems [83].

In the fluid phase, the incorporation of 20 mol% of TCV-116 does not alter the bilayer structure much. The data are satisfactorily fitted with the common bilayer model [40] (Fig. 4a and b, upper curves), and only a small reduction of the membrane thickness, d_{HH}, from 38.3 to 37.3 Å is observed (Fig. 5b, Table 2). This membrane thinning can be explained by the prodrug position in the monolayer leaflet (cp. Fig. 9). Since the overall penetration depth of TCV-116 is significantly smaller than the lipid monolayer thickness, one opposing DPPC–(TCV-116) pair in the bilayer is expected to span a shorter distance than two opposing lipids, and hence the overall membrane thickness reduces (see Fig. 5b and the schemes in Fig. 10). Obviously this effect gains in influence with increasing prodrug concentration, but it is for TCV-116 relatively small when compared to *e.g.* the membrane-thinning effect of valsartan. At a prodrug concentration of 20 mol% the membrane thickness decreases in fluid PC bilayers only 2–3% in the presence of candesartan cilexetil, whereas it reduces around 9% in the presence of valsartan. Also the estimated partial area per TCV-116 molecule is with about 46 Å^2 relatively small in comparison to the lipid area of DPPC (64 Å^2). This means that the partial interdigitation of lipids is hindered in the fluid phase and thus the membrane thinning is expected to be relatively small. In contrast, valsartan has a partial lateral area of 58 Å^2 [25] that comes close to the lipid area of DPPC. This favors partial interdigitation of DPPC lipids. Indeed the determined membrane thinning induced by 20 mol% valsartan is 3–4 times bigger as compared to the effect seen with candesartan cilexetil.

The observed increase in the intermembrane distances (Fig. 4, Table 2), especially in the gel-phase, can be explained by the negative surface charge density conferred to the bilayers upon TCV-116 insertion. Due to its acidic center at the tetrazole group (Fig. 1a) with a reported pK_a value of 5.9 [84] about 90% of the molecules are expected to be negatively ionized at neutral pH. This membrane repulsion force has also been reported for all other studied sartans [25,27,81,85]. Their effectiveness in unbinding membranes (*i.e.*, the electrostatic repulsion of neighboring membranes) depends solely on their pK_a values. Ranking the sartans in decreasing order of their pK_a values, reflects perfectly their membrane unbinding power, which increases in the order from TCV-116 → valsartan → irbesartan → olmesartan → losartan. While TCV-116 causes only a modest increase of the equilibrium distance between adjacent bilayers, losartan with the lowest pK_a (2.95–3.14 [20,84]) causes complete unbinding of the membranes, *i.e.*, the formation of unilamellar vesicles both in the gel and fluid phase of PCs [85].

4.3. Candesartan cilexetil's localization in lipid bilayers

MD calculations showed that prodrug TCV-116 prefers to locate in the interior of DPPC bilayers. Hereby, the prodrug is attached with its negatively charged tetrazole group with surrounding choline groups of the phospholipids, while its hydrophobic groups span the upper to middle segment of alkyl chains (Fig. 9a). Additionally, it exerts strong interaction with the DPPC–water interface through hydrogen bonds. A similar localization was observed also for other sartans [3,7,25–27,85].

This localization is expected due to the amphipathicity. For instance Siarhevera et al. showed using 2D NOESY ^{1}H–^{1}H MAS experiments that even structurally rather diverse molecules had all their highest concentration between the phosphate of the lipid headgroup and the upper segments of the lipid hydrocarbon chains. Thus, amphiphilic molecules are commonly localized in the same topography of lipid bilayers but still exerting different biological activity.

The firm anchoring of TCV-116 in DPPC bilayers is supported by ^{13}C CP/MAS experiments. The DPPC/TCV-116 bilayer spectra contain peaks with broad half-widths (Fig. 6). Such spectra are indicating reduced mobility in the system. As far as the AT_1 receptor antagonists are concerned a trend for the broadening of the peaks in the ^{13}C CP/MAS spectra could be identified: the bulkier the sartan is, the lower the bilayer mobility becomes [3,7,27].

The σ_{iso} and *brd* temperature profiles (Fig. 8a and c) derived from the simulations of the broadline ^{31}P NMR spectra (Fig. 7) provide information on the sartan localization in the DPPC bilayers due to the drug/membrane interactions. TCV-116 molecules clearly decrease significantly the isotropic chemical shift σ_{iso} due to the extra shielding provided to the ^{31}P of the headgroup. This indicates that TCV-116 molecules localize in the hydrophilic zone of the phospholipid bilayer formed by the polar headgroups and the lipid–water interface, in agreement with MD calculations (Fig. 9). Losartan insertion lowers the σ_{iso} values (Fig. 8a): (−21 ppm) [7] more than the candesartan [7] and TCV-116 molecules do (−20 ppm), indicating an even stronger interaction of losartan with the polar headgroup with respect to candesartan and TCV-116, at least in the liquid crystalline phase. This may be attributed to the fact that losartan has a lower pK_a value [20,84], *i.e.*, the fraction of negatively charged tetrazole groups is greater at neutral pH, and thus, losartan is interacting stronger with the positively charged choline groups of the surrounding DPPC lipids (cp. also the discussion on membrane unbinding in Section 4.2).

The values of *brd* in TCV-116 loaded DPPC bilayers are higher above 35 °C as compared to pure DPPC membranes (Fig. 8b), signifying that the incorporation of this sartan inhibits the bilayer mobility. Note, that this parameter is probably directly coupled to the measured chain mobility (see Raman ratio $I_{2935/2880}$ in Fig. 3C), which is also strongly reduced under the influence of TCV-116. Similar observations have been made for other studied sartans such as losartan and candesartan [7]. The decreased bilayer mobility of sartan loaded DPPC bilayers shows that drugs are localized close to the polar head moiety and affect the dipolar ^{1}H–^{31}P interaction of the phosphorus with the neighboring methylene protons. In the case of losartan, the *brd* values are continuously decreasing up to 50 °C (no clear sign of a pre- or main transition is apparent) reaching at about 50 °C the bilayer mobility of unloaded DPPC membranes (~2.5 ppm) [7]. In comparison CV-11974/DPPC [7] and TCV-116/DPPC bilayers display a slightly smaller bilayer mobility (~3.5 ppm) at 50 °C, indicating weaker dipolar ^{1}H–^{31}P interactions.

5. Conclusion and outlook

All AT_1 receptor antagonists studied so far are accommodated in the polar/apolar interface of the lipid bilayer. Such a localization for amphiphilic molecules is not surprising and has been for instance also reported for structurally rather diverse P-glycoprotein substrates [86]. The findings in this work provide significantly more information. The results from different complementary techniques (DSC, Raman spectroscopy, SAXS, WAXS, NMR, molecular modeling, and NMR simulation) are able to point out the complexity of the interactions of each individual AT_1 receptor antagonist with the plasma membrane.

(i) Each studied sartan causes more or less an electrostatic repulsion of neighboring membranes and its strength depends solely on its pK_a (referring to the acidic tetrazole group). Hence losartan displays the strongest intermembrane repulsion [85], while the here studied TCV-116 shows rather mild effects (Figs. 5c, 10).

(ii) As illustrated in Fig. 10D all studied sartans induce a bilayer thinning in the L_α phase. The most decisive parameter for the observed partial interdigitation of lipids is given in the partial molecular area of the sartans. We observed that sartans with molecular areas that come close to that of DPPC (64 $Å^2$) induce the strongest membrane thinning. For instance valsartan occupies an estimated molecular area of 58 $Å^2$ in DPPC bilayers and causes at 20 mol% drug concentration a thinning of 9% [25]. Contrarily the molecular area of TCV-116 covers only 46 $Å^2$ and consequently the membrane thinning effect (~1 Å) is rather small.

(iii) The majority of sartans induce the formation of drug rich and poor domains in the gel-phase regime. This concerns losartan [3,80], valsartan [25], irbesartan [81] and TCV-116 (this work). On the other hand, olmesartan [27] and the CV-11974 [7] do not induce any formation of drug-rich and drug-poor domains, *i.e.*, no splitting of the main transition is observed in the DSC-signal and the pre-transition gets only slightly disturbed.

(iv) All studied sartans except for olmesartan [27] decrease the fluidity (*gauche*/*trans* ratio) of the bilayers in the L_α phase. TCV-116 displays hereby the strongest effect of all so far studied sartans (Fig. 3a).

Even though most amphiphilic drugs are anchored in the lipid/water interface presumably maximizing their amphipathic interactions, they do not exert identical membrane perturbations, but as outlined above for the class of sartans, each drug is characterized in principle by its own individual "fingerprint". If we hypothesize that this fingerprint is essential for the drug's action, then future rational drug design should not only take into consideration direct drug action at the active site, but also the specific drug–bilayer interactions in order to forecast consequences in drug efficiency. This notion has been also adopted by other research groups for various classes of amphiphilic drug molecules [4,5,87–89]. In this respect a two step model was put forward for the action of AT_1 receptor antagonists reaching their active site by the "membrane pathway", and such, finding a suitable environment to exert their action [3,81].

Direct binding scenarios of sartans shall also be considered in future investigations. As outlined by Dror et al. in this binding pathway drugs encounter two major barriers: the "expected" barrier suggested by receptor geometry, proximal to the binding pocket, and also an "unexpected", earlier barrier at the receptor surface [90]. The early barrier is attributed to substantial drug–receptor dehydration that occurs far from the binding pocket. However, a comparison between the direct and the two-step "membrane pathway" has not been studied yet, but has triggered our interest. Therefore we have just initiated MD calculations to compare the preference of AT_1 receptor antagonists for one or the other pathway.

Acknowledgements

T. Mavromoustakos and D. Ntountaniotis acknowledge EAST-NMR program for covering the travel and residence expenses to perform NMR experiments in the Frankfurt solid state NMR Centre.

Appendix A. Supplementary data

Supplementary data to this article can be found online at http://dx.doi.org/10.1016/j.bbamem.2012.08.009.

References

[1] T. Mavromoustakos, A. Kolocouris, M. Zervou, P. Roumelioti, J.M. Matsoukas, R. Weisemann, An effort to understand the molecular basis of hypertension through the study of conformational analysis of losartan and sarmesin using a

combination of Nuclear Magnetic Resonance spectroscopy and theoretical calculations, J. Med. Chem. 42 (1999) 1714–1722.
[2] M. De Gasparo, K.J. Catt, T. Inagami, J.W. Wright, Th. Unger, International Union of Pharmacology. XXIII. The angiotensin II receptors, Pharmacol. Rev. 52 (2000) 415–472.
[3] P. Zoumpoulakis, I. Daliani, M. Zervou, I. Kyrikou, E. Siapi, G. Lamprinidis, E. Mikros, T. Mavromoustakos, Losartan's molecular basis of interaction with membranes and AT1 receptor, Chem. Phys. Lipids 125 (2003) 13–25.
[4] M. Lucio, J.L.F.C. Lima, S. Reis, Drug–membrane interactions: significance for medicinal chemistry, Curr. Med. Chem. 17 (2010) 1795–1809.
[5] A.M. Seddon, D. Casey, R.V. Law, A. Gee, R.H. Templer, O. Ces, Drug interactions with lipid membranes, Chem. Soc. Rev. 38 (2009) 2509–2519.
[6] L.J. Wagenaar, A.A. Voors, H. Buikema, A. Van Buiten, R.H. Lübeck, P.W. Boonstra, D.J. Van Veldhuisen, W.H. Van Gilst, Functional antagonism of different angiotensin II type I receptor blockers in human arteries, Cardiovasc. Drugs Ther. 16 (2002) 311–316.
[7] C. Fotakis, D. Christodouleas, P. Zoumpoulakis, E. Kritsi, N.P. Benetis, T. Mavromoustakos, H. Reis, A. Gili, M.G. Papadopoulos, M. Zervou, Comparative biophysical studies of sartan class drug molecules losartan and candesartan (CV-11974) with membrane bilayers, J. Phys. Chem. B 115 (2011) 6180–6192.
[8] T.R. Oliveira, M.T. Lamy, U.M. De Paula, L.L. Guimarães, M.S. Toledo, H.K. Takahashi, A.H. Straus, C.J. Lindsey, T.B. Paiva, Structural properties of lipid reconstructs and lipid composition of normotensive and hypertensive rat vascular smooth muscle cell membranes, Braz. J. Med. Biol. Res. 42 (2009) 844–853.
[9] T.J. Netticadan, T.F. Ashavaid, K.G. Nair, Characterisation of the canine cardiac sarcolemma in experimental myocardial ischemia, Indian J. Clin. Biochem. 12 (1997) 49–54.
[10] R. Koynova, M. Caffrey, Phases and phase transitions of the phosphatidylcholines, Biochim. Biophys. Acta 1376 (1998) 91–145.
[11] S. Tristram-Nagle, M.C. Wiener, C.P. Yang, J.F. Nagle, Kinetics of the subtransition in dipalmitoylphosphatidylcholine, Biochemistry 26 (1987) 4288–4294.
[12] M.D. Housley, K.K. Stanley, Dynamics of Biological Membranes, John Wiley and Sons, New York, 1982.
[13] R.P. Rand, D. Chapman, K. Larsson, Tilted hydrocarbon chains of dipalmitoyl lecithin become perpendicular to the bilayer before melting, Biophys. J. 15 (1975) 1117–1124.
[14] J. Stamatoff, B. Feuer, H.J. Guggenheim, G. Tellez, T. Yamane, Amplitude of rippling in the P beta phase of dipalmitoylphosphatidylcholine bilayers, Biophys. J. 38 (1982) 217–226.
[15] T.J. McIntosh, Differences in hydrocarbon chain tilt between hydrated phosphatidylethanolamine and phosphatidylcholine bilayer. A molecular packing model, Biophys. J. 29 (1980) 237–245.
[16] N.B. Colthulp, L.H. Daly, S.E. Wiberley, Introduction to Infrared and Raman Spectroscopy, Academic Press, 1990.
[17] C.H. Huang, J.R. Lapides, I.W. Levin, Phase-transition behaviour of saturated, symmetric chain phospholipid bilayers dispersions determined by Raman spectroscopy: correlation between spectral and thermodynamic parameters, J. Am. Chem. Soc. 104 (1982) 5926–5930.
[18] I.W. Levin, R.N. Lewis, Fourier transform Raman spectroscopy of biological materials, Anal. Chem. 62 (1990) 1101A–1111A.
[19] G. Pabst, M. Rappolt, H. Amenitsch, P. Laggner, Structural information from multilamellar liposomes at full hydration: full q-range fitting with high quality X-ray data, Phys. Rev. E 62 (2000) 4000–4009.
[20] P. Tosco, B. Rolando, R. Fruttero, Y. Henchoz, S. Martel, P.A. Carrupt, A. Gasco, Physicochemical profiling of sartans: a detailed study of ionization constants and distribution coefficients, Helv. Chim. Acta 91 (2008) 468–482.
[21] A. Ramamoorthy, Beyond NMR spectra of antimicrobial peptides: dynamical images at atomic resolution and functional insights, Solid State Nucl. Magn. Reson. 35 (2009) 201–207.
[22] H. Jerebek, G. Pabst, M. Rappolt, T. Stockner, Membrane-mediated effect on ion channels induced by the anesthetic drug ketamine, J. Am. Chem. Soc. 132 (2010) 7990–7997.
[23] R.S. Cantor, Lipid composition and the lateral pressure profile in bilayers, Biophys. J. 76 (1999) 2625–2639.
[24] C. Xing, O.H.S. Ollila, I. Vattulainen, R. Faller, Asymmetric nature of lateral pressure profiles in supported lipid membranes and its implications for membrane protein functions, Soft Matter 5 (2009) 3258–3261.
[25] C. Potamitis, P. Chatzigeorgiou, E. Siapi, K. Viras, T. Mavromoustakos, A. Hodzic, G. Pabst, F. Cacho-Nerin, P. Laggner, M. Rappolt, Interactions of the AT1 antagonist valsartan with dipalmitoyl-phosphatidylcholine bilayers, Biochim. Biophys. Acta 1808 (2011) 1753–1763.
[26] C. Fotakis, D. Christodouleas, P. Chatzigeorgiou, M. Zervou, N.-P. Benetis, K. Viras, T. Mavromoustakos, Development of a CP 31P NMR broadline simulation methodology for studying the interactions of antihypertensive AT1 antagonist losartan with phospholipid bilayers, Biophys. J. 96 (2009) 2227–2236.
[27] D. Ntountaniotis, G. Mali, S.G. Grdadolnik, M. Halabalaki, A.-L. Skaltsounis, C. Potamitis, E. Siapi, P. Chatzigeorgiou, M. Rappolt, T. Mavromoustakos, Thermal, dynamic and structural properties of drug AT1 antagonist olmesartan in lipid bilayers, Biochim. Biophys. Acta 1808 (2011) 2995–3006.
[28] I. Kyrikou, N.P. Benetis, P. Chatzigeorgiou, M. Zervou, K. Viras, C. Poulos, T. Mavromoustakos, Interactions of the dipeptide paralysin β-Ala-Tyr and the aminoacid Glu with phospholipid bilayers, Biochim. Biophys. Acta 1778 (2008) 113–124.
[29] T.M. Mavromoustakos, The use of differential scanning calorimetry to study drug–membrane interactions, Meth. Mol. Biol. 400 (2007) 587–600.
[30] A. Hodzic, M. Rappolt, H. Amenitsch, G. Pabst, Differential modulation of membrane structure and fluctuations by plant sterols and cholesterol, Biophys. J. 94 (2008) 3935–3944.
[31] T. Mavromoustakos, P. Chatzigeorgiou, C. Koukoulitsa, S. Durdagi, Partial interdigitation of lipid bilayers, Int. J. Quantum Chem. 111 (2011) 1172–1183.
[32] U. Holzgrabe, I. Wawer, B. Diehl, NMR Spectroscopy in Pharmaceutical Analysis, Elsevier, Amsterdam, 2008.
[33] C. Song, H. Holmsen, W. Nerdal, Existence of lipid microdomains in bilayer of dipalmitoyl phosphatidylcholine (DPPC) and 1-stearoyl-2-docosahexenoyl phosphatidylserine (SDPS) and their perturbation by chlorpromazine: a 13C and 31P solid-state NMR study, Biophys. Chem. 120 (2006) 178–187.
[34] T. Mavromoustakos, I. Daliani, Effects of cannabinoids in membrane bilayers containing cholesterol, Biochim. Biophys. Acta 1420 (1999) 252–265.
[35] T. Mavromoustakos, E. Theodoropoulou, A combined use of 13C-cross polarization/magic angle spinning, 13C-magic angle spinning and 31P-nuclear magnetic resonance spectroscopy with differential scanning calorimetry to study cannabinoid–membrane interactions, Chem. Phys. Lipids 92 (1998) 37–52.
[36] C. Fotakis, S. Gega, E. Siapi, C. Potamitis, K. Viras, P. Moutevelis-Minakakis, C.G. Kokotos, S. Durdagi, S. Golic Grdadolnik, B. Sartori, M. Rappolt, T. Mavromoustakos, Interactions at the bilayer interface and receptor site induced by the novel synthetic pyrrolidinone analog MMK3, Biochim. Biophys. Acta 1768 (2010) 422–432.
[37] H. Amenitsch, M. Rappolt, M. Kriechbaum, H. Mio, P. Laggner, S. Bernstorff, First performance assessment of the small-angle X-ray scattering beamline at ELETTRA, J. Synchrotron Radiat. 5 (1998) 506–508.
[38] A. Caillé, Remarques sur la diffusion des rayons X dans les smectiques A, C. R. Acad. Sci. Paris B 274 (1972) 891–893.
[39] R. Zhang, S. Tristram-Nagle, W. Sun, R.L. Headrick, T.C. Irving, R.M. Suter, J.F. Nagle, Small-angle X-ray scattering from lipid bilayers is well described by modified Caillé theory but not by paracrystalline theory, Biophys. J. 70 (1996) 349–357.
[40] M. Rappolt, Bilayer thickness estimations with "poor" diffraction data, J. Appl. Phys. 107 (2010) 084701-1–084701-7.
[41] J.F. Nagle, S. Tristram-Nagle, Structure and interactions of lipid bilayer: role of fluctuations, in: J. Katsaras, T. Gutberlet (Eds.), Lipid Bilayers. Structure and Interactions, Springer, Berlin, 2000, pp. 1–23.
[42] J.F. Nagle, S. Tristram-Nagle, Structure of lipid bilayers, Biochim. Biophys. Acta 1469 (2000) 159–195.
[43] S.W. Chiu, E. Jakobsson, R.J. Mashl, H.L. Scott, Cholesterol-induced modifications in lipid bilayers: a simulation study, Biophys. J. 83 (2002) 1842–1853.
[44] J.J.P. Stewart, Application of the PM6 method to modeling the solid state, J. Mol. Model. 14 (2008) 499–535.
[45] J.J.P. Stewart, Optimization of parameters for semiempirical methods V: modification of NDDO approximations and application to 70 elements, J. Mol. Model. 13 (2007) 1173–1213.
[46] G. Melagraki, A. Afantitis, H. Sarimveis, P.A. Koutentis, G. Kollias, O. Igglessi-Markopoulou, Predictive QSAR workflow for the in silico identification and screening of novel HDAC inhibitors, Mol. Divers. 13 (2009) 301–311.
[47] T. Puzyn, N. Suzuki, M. Haranczyk, J. Rak, Calculation of quantum-mechanical descriptors for QSPR at the DFT level: is it necessary? J. Chem. Inf. Model. 48 (2008) 1174–1180.
[48] A. Klamt, G. Schüürmann, COSMO: a new approach to dielectric screening in solvents with explicit expressions for the screening energy and its gradient, J. Chem. Soc., Perkin Trans. 2 (1993) 799–805.
[49] J.S. Puranen, M.J. Vainio, M.S. Johnson, Accurate conformation-dependent molecular electrostatic potentials for high-throughput in silico drug discovery, J. Comput. Chem. 31 (2010) 1722–1732.
[50] J.B. Klauda, R.M. Venable, J.A. Freites, J.W. O'Connor, D.J. Tobias, C. Mondragon-Ramirez, I. Vorobyov, J. MacKerell, R.W. Pastor, Update of the CHARMM all-atom additive force field for lipids: validation on six lipid types, J. Phys. Chem. B 114 (2010) 7830–7843.
[51] R.W. Pastor, A.D. MacKerell, Development of the CHARMM force field for lipids, J. Phys. Chem. Lett. 2 (2011) 1526–1532.
[52] W.L. Jorgensen, J. Chandrasekhar, J.D. Madura, R.W. Impey, M.L. Klein, Comparison of simple potential functions for simulating liquid water, J. Chem. Phys. 79 (1983) 926–935.
[53] V. Zoete, M.A. Cuendet, A. Grosdidier, O. Michielin, SwissParam: a fast force field generation tool for small organic molecules, J. Comput. Chem. 32 (2011) 2359–2368.
[54] B. Hess, C. Kutzner, D. van der Spoel, E. Lindahl, GROMACS 4: algorithms for highly efficient, load-balanced, and scalable molecular simulation, J. Chem. Theory Comput. 4 (2008) 435–447.
[55] T.A. Halgren, Merck molecular force field. I. Basis, form, scope, parameterization, and performance of MMFF94, J. Comput. Chem. 17 (1996) 490–519.
[56] H.J.C. Berendsen, J.P.M. Postma, W.F. Van Gunsteren, A. Dinola, J.R. Haak, Molecular dynamics with coupling to an external bath, J. Chem. Phys. 81 (1984) 3684–3690.
[57] U. Essmann, L. Perera, M.L. Berkowitz, T. Darden, H. Lee, L.G. Pedersen, A smooth particle mesh Ewald method, J. Chem. Phys. 103 (1995) 8577–8593.
[58] S. Kumar, J.M. Rosenberg, D. Bouzida, R.H. Swendsen, P.A. Kollman, The weighted histogram analysis method for free-energy calculations on biomolecules. I. The method, J. Comput. Chem. 13 (1992) 1011–1021.
[59] J.S. Hub, B.L. De Groot, D. van der Spoel, G-whams—a free Weighted Histogram Analysis implementation including robust error and autocorrelation estimates, J. Chem. Theory Comput. 6 (2010) 3713–3720.
[60] E.B. Kim, N. Lockwood, M. Chopra, O. Guzmán, N.L. Abbott, J.J. De Pablo, Interactions of liquid crystal-forming molecules with phospholipid bilayers studied by molecular dynamics simulations, Biophys. J. 89 (2005) 3141–3158.
[61] J.A. Lemkul, D.R. Bevan, Assessing the stability of Alzheimer's amyloid protofibrils using molecular dynamics, J. Phys. Chem. B 114 (2010) 1652–1660.
[62] E.F. Pettersen, T.D. Goddard, C.C. Huang, G.S. Couch, D.M. Greenblatt, E.C. Meng, T.E. Ferrin, UCSF Chimera—a visualization system for exploratory research and analysis, J. Comput. Chem. 25 (2004) 1605–1612.

[63] R.K. Bista, R.F. Bruch, A.M. Covington, Variable-temperature Raman spectromicroscopy for a comprehensive analysis of the conformational order in PEGylated lipids, J. Raman Spectrosc. 40 (2008) 463–471.
[64] J.R. Silvius, M. Lyons, P.L. Yeagle, T.J. O'Leary, Thermotropic properties of bilayers containing blanched-chain phospholipids, calorimetric, Raman and 31P NMR studies, Biochemistry 24 (1985) 5388–5395.
[65] T.J. O'Leary, P.D. Ross, I.W. Levin, Effects of anesthetic and nonanesthetic steroids on dipalmitoylphosphatidylcholine liposomes: a calorimetric and Raman spectroscopic investigation, Biochemistry 23 (1984) 4636–4641.
[66] T.J. O'Leary, I.W. Levin, Raman spectroscopic study of an interdigitated lipid bilayer dipalmitoylphosphatidylcholine dispersed in glycerol, Biochim. Biophys. Acta 776 (1984) 185–189.
[67] R. Hosemann, S.N. Bagchi, Direct Analysis of Diffraction by Matter, North-Holland Publ. Co., Amsterdam, 1962.
[68] H.I. Petrache, N. Gouliaev, S. Tristram-Nagle, R.T. Zhang, R.M. Suter, J.F. Nagle, Interbilayer interactions from high-resolution X-ray scattering, Phys. Rev. E 57 (1998) 7014–7024.
[69] W.J. Sun, R.M. Suter, M.A. Knewtson, C.R. Worthington, S. Tristram-Nagle, R. Zhang, J.F. Nagle, Order and disorder in fully hydrated unoriented bilayers of gel phase dipalmitoylphosphatidylcholine, Phys. Rev. E 49 (1994) 4665–4676.
[70] K.P. Soteriadou, A.K. Tzinia, E. Panou-Pamonis, V. Tsikaris, M. Sakarellos-Daitsiotis, C. Sakarellos, Y. Papapoulou, R. Matsas, Antigenicity and conformational analysis of the Zn2+-binding sites of two Zn2+-metalloproteases: *Leishmania* gp63 and mammalian endopeptidase-24.11, Biochem. J. 313 (1996) 455–466.
[71] P. Zoumpoulakis, S.G. Grdadolnik, J.M. Matsoukas, T. Mavromoustakos, Structure elucidation and conformational properties of eprosartan a non peptide Angiotensin II AT1 antagonist, J. Pharm. Biomed. Anal. 28 (2002) 125–135.
[72] P. Zoumpoulakis, A. Zoga, P. Roumelioti, N. Giatas, S.G. Grdadolnik, E. Iliodromitis, D. Vlahakos, D. Kremastinos, J.M. Matsoukas, T. Mavromoustakos, Conformational and biological studies for a pair of novel synthetic AT1 antagonists. Stereoelectronic requirements for antihypertensive efficacy, J. Pharm. Biomed. Anal. 31 (2003) 833–844.
[73] P. Zoumpoulakis, A. Politi, S.G. Grdadolnik, J.M. Matsoukas, T. Mavromoustakos, Structure elucidation and conformational study of V8. A novel synthetic non peptide AT1 antagonist, J. Pharm. Biomed. Anal. 40 (2006) 1097–1104.
[74] C. Neale, W.F.D. Bennett, D.P. Tieleman, R. Pomes, Statistical convergence of equilibrium properties in simulations of molecular solutes embedded in lipid bilayers, J. Chem. Theory Comput. 7 (2011) 4175–4188.
[75] G. Pabst, H. Amenitsch, D.P. Kharakoz, P. Laggner, M. Rappolt, Structure and fluctuations of phosphatidylcholines in the vicinity of the main phase transition, Phys. Rev. E 70 (2004) 021908-1–021908-9.
[76] J.F. Nagle, D.A. Wilkinson, Lecithin bilayers. Density measurements and molecular interactions, Biophys. J. 23 (1978) 159–175.
[77] T. Heimburg, A model for the lipid pretransition: coupling of ripple formation with the chain-melting transition, Biophys. J. 78 (2000) 1154–1165.
[78] M. Rappolt, G. Pabst, G. Rapp, M. Kriechbaum, H. Amenitsch, C. Krenn, S. Bernstorff, P. Laggner, New evidence for gel-liquid crystalline phase coexistence in the ripple phase of phosphatidylcholines, Eur. Biophys. J. 29 (2000) 125–133.
[79] K. Sengupta, V.A. Raghunathan, J. Katsaras, Novel structural features of the ripple phase of phospholipids, Europhys. Lett. 49 (2000) 722–728.
[80] E. Theodoropoulou, D. Marsh, Interactions of angiotensin II non-peptide AT1 antagonist losartan with phospholipid membranes studied by combined use of differential scanning calorimetry and electron spin resonance spectroscopy, Biochim. Biophys. Acta 1461 (1999) 135–146.
[81] T. Mavromoustakos, P. Zoumpoulakis, I. Kyrikou, A. Zoga, E. Siapi, M. Zervou, I. Daliani, D. Dimitriou, A. Pitsasa, C. Kamoutsis, P. Laggner, Efforts to understand the molecular basis of hypertension through drug:membrane interactions, Curr. Top. Med. Chem. 4 (2004) 445–459.
[82] M.J. Ruocco, G.G. Shipley, Characterization of the sub-transition of hydrated dipalmitoylphosphatidylcholine bilayers. Kinetic, hydration and structural study, Biochim. Biophys. Acta 691 (1982) 309–320.
[83] E.S. Rowe, T.A. Cutrera, Differential scanning calorimetric studies of ethanol interactions with distearoylphosphatidylcholine: transition to the interdigitated phase, Biochemistry 29 (1990) 10398–10404.
[84] E. Cagigal, L. Gonzalez, R.M. Alonso, R.M. Jimenez, pKa determination of angiotensin II receptor antagonists (ARA II) by spectrofluorimetry, J. Pharm. Biomed. Anal. 26 (2001) 477–486.
[85] A. Hodzic, P. Zoumpoulakis, G. Pabst, T. Mavromoustakos, M. Rappolt, Losartan's affinity to fluid bilayers modulates lipid–cholesterol interactions, Phys. Chem. Chem. Phys. 14 (2012) 4780–4788.
[86] A. Siarheyeva, J.J. Lopez, C. Glaubitz, Localization of multidrug transporter substrates within model membranes, Biochemistry 45 (2006) 6203–6211.
[87] X. Tian, S. Pavlopoulos, D.P. Yang, A. Makriyannis, The interaction of cannabinoid receptor agonists, CP55940 and WIN55212-2 with membranes using solid state 2H NMR, Biochim. Biophys. Acta Biomembr. 1808 (2011) 2095–2101.
[88] D.G. Rhodes, J.G. Sarmiento, L.G. Herbette, The “membrane bilayer” pathway, Mol. Pharmacol. 27 (1985) 612–623.
[89] D.P. Hurst, A. Grossfield, D.L. Lynch, S. Feller, T.D. Romo, K. Gawrisch, M.C. Pitman, P.H. Reggio, A lipid pathway for ligand binding is necessary for a cannabinoid G protein-coupled receptor, J. Biol. Chem. 285 (2010) 17954–17964.
[90] R.O. Dror, A.C. Pan, D.H. Arlow, D.W. Borhani, P. Maragakis, Y. Shan, H. Xu, D.E. Shaw, Pathway and mechanism of drug binding to G-protein-coupled receptors, Proc. Natl. Acad. Sci. U. S. A. 108 (2011) 13118–13123.